Coulomb excitation of ^{102}Ru with ^{12}C and ^{16}O

P. E. Garrett,[1,2] M. Zielińska,[3] A. Bergmaier,[4] T. R. Rodríguez,[5] D. Kalaydjieva,[3] M. Siciliano,[6] H. Bidaman,[1]
V. Bildstein,[1] C. Burbadge,[1] A. Diaz Varela,[1] D. T. Doherty,[7] T. Faestermann,[8] K. Hadyńska-Klęk,[7,*] R. Hertenberger,[9]
N. Keeley,[10] A. Laffoley,[1] A. D. MacLean,[1] M. Mahgoub,[11,12] A. J. Radich,[1] M. Rocchini,[1] P. Spagnoletti,[13]
S. Triambak,[2] M. Vandebrouck,[3] and K. Wrzosek-Lipska[14]

[1]*Department of Physics, University of Guelph, Guelph, Ontario, N1G2W1 Canada*
[2]*Department of Physics and Astronomy, University of the Western Cape, P/B X17, Bellville ZA-7535, South Africa*
[3]*IRFU, CEA, Université Paris-Saclay, 91191 Gif-sur-Yvette, France*
[4]*Institut für Angewandte Physik und Messtechnik (LRT2), Fakultät für Luft- und Raumfahrttechnik,
Universität der Bundeswehr München, D-85577 Neubiberg, Germany*
[5]*Departamento de Física Teórica and CIAFF, Universidad Autónoma de Madrid, E-28049 Madrid, Spain*
[6]*Physics Division, Argonne National Laboratory, Argonne, Illinois 60439, USA*
[7]*Department of Physics, University of Surrey, Guildford GU2 7XH, United Kingdom*
[8]*Physik Department, Technische Universität München, D-85748 Garching, Germany*
[9]*Fakultät für Physik, Ludwig-Maximilians-Universität München, D-85748 Garching, Germany*
[10]*National Centre for Nuclear Research, Sołtana 7, PL-05-400 Otwock, Poland*
[11]*Physics Department, Jazan University, 45142 Jazan, Saudi Arabia*
[12]*Department of Physics, Sudan University of Science and Technology, PO Box 407, Khartoum, Sudan*
[13]*University of the West of Scotland, Paisley PA1 2BE, United Kingdom*
[14]*Heavy Ion Laboratory, University of Warsaw, Pasteura 5a, 02-093 Warsaw, Poland*

The Coulomb excitation of ^{102}Ru was performed with beams of ^{12}C and ^{16}O ions. The beam particles scattered at forward angles were momentum analyzed with a magnetic spectrograph. The resolution achieved enabled the populations of the 2_1^+ state, the unresolved $2_2^+/4_1^+$, and $2_4^+/3_1^-$, doublets of states, and the 3_2^- state to be determined as a function of the scattering angle. These populations are compared with GOSIA calculations, yielding $B(E2; 2_1^+ \rightarrow 0_1^+) = 41.5 \pm 2.3$ W.u., $B(E2; 2_2^+ \rightarrow 0_1^+) = 1.75 \pm 0.11$ W.u., $B(E3; 3_1^- \rightarrow 0_1^+) = 31.5 \pm 3.5$ W.u., and $B(E3; 3_2^- \rightarrow 0_1^+) = 6.8 \pm 0.5$ W.u. The $B(E3; 3_1^- \rightarrow 0_1^+)$ value is significantly larger than previously measured. The weakly populated 2_3^+ state, presumed to be a member of the band built on the 0_2^+ state, was observed clearly for a single angle only, and a fit to its population results in $B(E2; 2_3^+ \rightarrow 0_1^+) = 0.053 \pm 0.011$ W.u. Using the known γ-ray branching ratios for the 2_3^+ level, the $B(E2; 2_3^+ \rightarrow 0_2^+)$ value is calculated to be 18 ± 4 W.u., substantially less than the $B(E2; 2_1^+ \rightarrow 0_1^+)$. This suggests that the deformation of the 0_2^+ state is lower than that of the 0_1^+ state. The results are compared with beyond-mean-field calculations with the Gogny-D1S interaction using the symmetry-conserving configuration-mixing method.

I. INTRODUCTION

The nucleus ^{102}Ru has been described as "pivotal for the $A \simeq 100$ region" [1] based on its presumed placement as marking a boundary in Z between nuclei that become deformed with increasing N, such as the Sr, Zr, and Mo isotopes, and also marking a boundary in N of nuclei that exhibit a phase transition mediated by the underlying sub-shell structure, as the above nuclei have rapid changes in the ground-state structure at $N = 60$. This is reflected in the excitation energies plotted in Fig. 1; rapid decreases in the excitation energies of the 2_1^+ states are observed between

the $N = 58$ and $N = 60$ Sr, Zr, and to a lesser extent the Mo isotopes, whereas the Ru isotopes follow a smoother evolution. The excitation energies of the 0_2^+ states in the Sr and Zr isotopes also present sudden changes, with their extremely low energies observed at $N = 60$, whereas in the Mo isotopes the 0_2^+ states have rather constant low energies for $56 \leqslant N \leqslant 60$. In the Ru isotopes, the lowest 0_2^+ energy occurs in the $N = 58$ ^{102}Ru at 944 keV, and the behavior of the energy systematics surrounding this point is perhaps best described as intermediate between the Pd and Mo isotopes.

The structures of the Ru isotopes in the vicinity of $N = 58$ have been interpreted in a variety of ways. The systematics of the 2_1^+ energies, and the $E(4_1^+)/E(2_1^+)$ energy ratios, have been used to suggest an evolution from a spherical vibrational scheme for the lighter Ru isotopes (^{96,98}Ru) to that of a γ-soft rotor for the heavier ones (^{106,108}Ru), or, in the language of
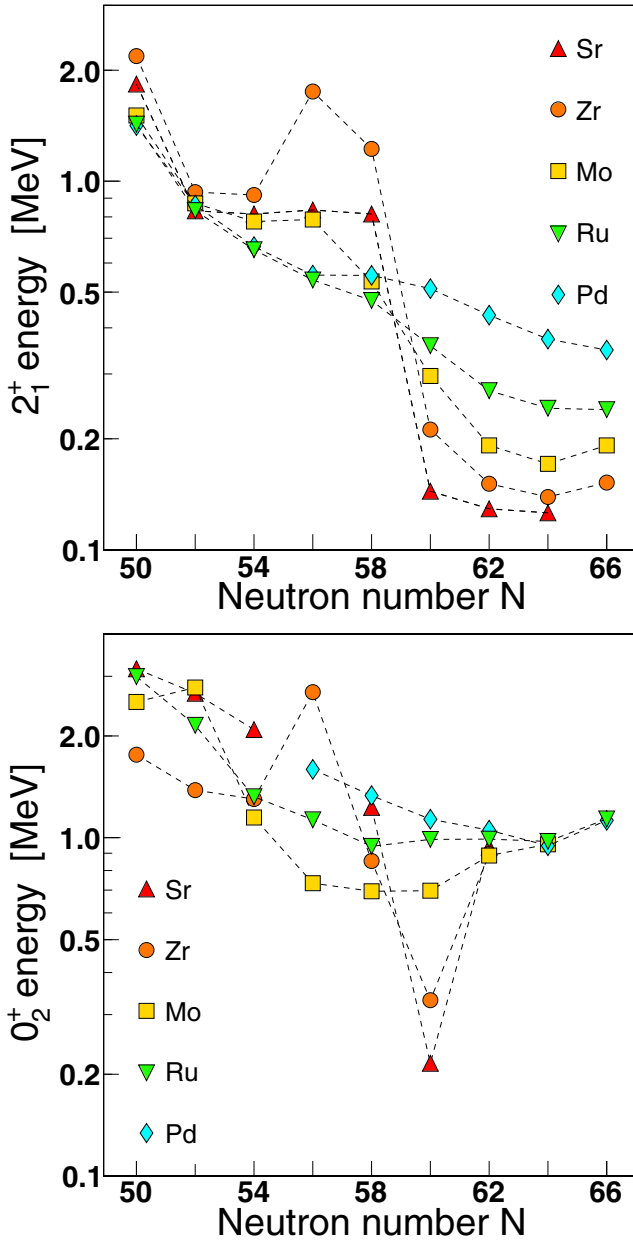
FIG. 1. Systematics of the 2_1^+ energies (top) and 0_2^+-state energies (bottom) for the Zr, Sr, Mo, Ru, and Pd isotopes.

the interacting boson model (IBM), structures that are intermediate between the U(5) and SO(6) limits [2–6]. Early work [7] predicted that the heavier Ru isotopes ^{106,108,110}Ru were soft in both the β_2 and γ shape degree of freedom, and work by Faessler *et al.* [8] predicted a change in the ground-state deformation occurring between ^{98}Ru ($\beta_2 = 0$) and ^{100}Ru ($\beta_2 = 0.17$, $\gamma = 20°$), with the heavier Ru isotopes becoming increasingly deformed and maximally triaxial. In a Coulomb-excitation study of ^{104}Ru by Stachel *et al.* [9], it was suggested that the 0_2^+ state was not the first-excited 0^+ state predicted by collective models, but rather was built on an "intruder" configuration with a smaller deformation and higher degree of triaxiality than the ground state. The suggestion of the special natures of the 0_2^+ states in ^{104,106}Ru was reinforced

with the observation that they were strongly populated in the (t, p) reaction [10], with strengths approximately 20% of those of the ground state. Large strengths were also observed in the ^{98,100}Mo(t, p) reactions [10,11] for the populations of the 0_2^+ states, perhaps indicating a structural similarity, but in the ^{96}Mo(t, p) reaction the 0_2^+ state was weakly populated [11]. The $(^3$He, $n)$ two-proton transfer reaction, on the other hand, produced no observable population for excited states in ^{102}Ru, whereas the 0_2^+ state in ^{98}Ru was populated with 13% of the ground-state cross section [12]. These results point to changing natures of the configurations as a function of the neutron number in the Mo and Ru isotopes.

Shape coexistence in the Ru isotopes with $A \geqslant 100$ was predicted by Troltenier *et al.* [13] using the general collective model, with two minima predicted in the potential-energy surfaces (PES); one spherical, and one triaxial with $(\beta_2, \gamma) \approx (0.42, 24°)$. The gradual shape change in the ground state of the Ru isotopes, in contrast with the rapid change observed in the Sr and Zr isotopes, was explained [14] as being due to the occupancy of the $\pi g_{9/2}$ orbitals that largely block the promotion of the protons from the lower $1p0f$ orbitals. More recent studies employed Hartree-Fock-Bogoliubov calculations with a Gogny-D1M energy density functional, followed by a mapping procedure onto the IBM-1 Hamiltonian to investigate the spectroscopic properties of Ru, Mo, Zr, and Sr nuclei [15]. These calculations predicted that many of the Ru isotopes exhibited γ softness, but their potential-energy surfaces did not possess coexisting minima. Other calculations using relativistic Hartree-Bogoliubov formalism with density-dependent zero- and finite-range nucleon-nucleon interactions found that shape coexistence did not manifest in any Ru isotope except ^{104}Ru [16]. Beyond-mean-field calculations employing the five-dimensional collective Hamiltonian with parameters determined by constrained self-consistent mean-field calculations based on the relativistic energy density functional PC-PK1 predicted that ^{100}Ru was nearly prolate, with a global minimum in the PES at $(0.22, 4°)$, and ^{102}Ru had a triaxial minimum at $\gamma = 19°$ and was also predicted to be rather γ soft [17]. The PESs for ^{104,106}Ru were somewhat similar [17]. The Ru isotopes have also been considered in the context of lying at a critical point of a shape phase transition, with ^{104}Ru postulated as a candidate for $E(5)$ symmetry [18], and ^{100}Ru at the critical point for the U(5)-SO(6) transition [19].

The band built on the 0_2^+ state in ^{102}Ru was identified by Urban *et al.* [20] using the (n, γ) reaction. Based on the known systematics at the time, it was suggested [20] that there are two relatively unperturbed configurations for the 0^+ states at $N = 52$ which evolve differently with N. The first configuration formed the ground state in ^{96}Ru that has a nearly spherical shape, and its deformation was suggested to remain approximately constant with N. At $N = 60$ and beyond this configuration would correspond to the excited 0_2^+ state. The second configuration would be that of the 0_2^+ state in ^{96}Ru, and it was also suggested to possess low deformation. However, unlike the 0_1^+ state, the 0_2^+ state's deformation was postulated to increase with N, and the crossing of the two configurations would occur at ^{100,102}Ru. The deformed second configuration would become the ground state in ^{104}Ru. As a result of the

mixing near the crossing, both 0^+ states take on deformed characteristics. A recent study [21,22] combining the use of γ-ray spectroscopy following the β decay of ^{98}Rh and the ^{100}Ru(p,t) ^{98}Ru reaction identified the 0_2^+ and "γ" bands in ^{98}Ru which fit well in the systematics of these excitations in the heavier Ru isotopes. It was noted that the energy spacings of states in the excited 0_2^+ band in ^{98}Ru bore a strong similarity to those of the ground-state band in ^{102}Ru, and from a two-band-mixing analysis it was suggested [21] that the configuration crossing occurs between ^{98}Ru and ^{100}Ru. Beyond-mean-field calculations employing the symmetry-conserving configuration mixing (SCCM) method with the Gogny-D1S functional for the interaction were performed [21], and the results pointed to shape coexistence occurring as the deformation evolves along the Ru isotope chain from ^{96}Ru to ^{106}Ru. Shape coexistence has been firmly established experimentally in the neighboring ^{98,100}Mo isotopes [23,24]. In the Ru isotopes, the most detailed investigation of nuclear shapes resulted from a series of Coulomb-excitation experiments for ^{104}Ru [25] that progressed beyond the earlier study [9] and yielded a large set of transitional and diagonal matrix elements which enabled rather precise determinations of the invariant quantities $\langle Q^2 \rangle$ and $\langle Q^3 \cos 3\delta \rangle$ for multiple states. For the ground-state band members, their values are approximately constant up to the 8_1^+ level with $\langle Q^2 \rangle \approx 0.9~e^2\,\mathrm{b}^2$, corresponding to $\beta_2 \approx 0.28$, and the variance for the ground state was $\sigma(Q^2) \approx 0.22(6)$ [25], indicating some dispersion in $\langle Q^2 \rangle$ but with definite static deformation; the diagonal matrix elements for the ground-state band were also constant within experimental uncertainty with a value of $-0.71(11)$ e b for the 2_1^+ state. The values of $\langle \cos 3\delta \rangle$ evolve from slightly less than 0.4 for the ground state to slightly greater than 0.45 for the 8_1^+ level, corresponding to a triaxial shape with $\gamma \approx 25°$ [25]. For the 0_2^+ level, $\langle Q^2 \rangle = 0.52(12)~e^2\,\mathrm{b}^2$ ($\beta_2 \approx 0.21$), indicating substantially smaller deformation [25], and $\langle \cos 3\delta \rangle = 0.1(3)$. While the uncertainty on the latter quantity is large, it is also indicative of a triaxial shape. Unfortunately, the dispersion in these quantities could not be extracted.

Aside from purely structural interest, the Ru isotopes are parent (^{96}Ru) or daughter (^{100,102}Ru) candidates for searches for the $0\nu\beta\beta$ process. The NEMO-3 collaboration recently published [26] the most precise $2\nu\beta\beta$ measurements to date for the decay of ^{100}Mo to the ground state of ^{100}Ru, with a half-life of $t_{1/2} = [6.81 \pm 0.01(\mathrm{stat})^{+0.38}_{-0.40}(\mathrm{sys})] \times 10^{18}$ years, as well as the two-electron energy sum, the single-electron energy spectra, and the angular correlation of the two emitted electrons [26]. The $2\nu\beta\beta$ decay has also been observed [27] to proceed to the excited 0_2^+ state of ^{100}Ru at 1130 keV with a measured half-life of $t_{1/2} = (6.1^{+1.8}_{-1.1}) \times 10^{20}$ years, or a factor of approximately 100 times longer than the ground-state decay. Limits on the double-β decay of ^{102}Pd to the excited 2_1^+ ($t_{1/2} > 5.95 \times 10^{18}$ yr), 0_2^+ ($t_{1/2} > 5.81 \times 10^{18}$ yr), and 2_2^+ ($t_{1/2} > 8.55 \times 10^{18}$ yr) states have been established [28]. While the half-lives for decay to excited states are typically much longer, they potentially offer promise due to the experimental ability to apply a condition on the deexciting γ rays. The $2\nu\beta\beta$ mode serves as a benchmark for calculations of the nuclear matrix elements that are critical for the

$0\nu\beta\beta$ process, and the role that deformation effects have on the nuclear matrix elements has been emphasized [29]. Deformation effects have been widely explored with different many-body methods, and it was found that there is an anticorrelation between the nuclear matrix elements, and the change in the deformation between the parent and daughter state. Thus, knowledge on both ground-state and excited-state deformations are important if such processes were to yield an observable double-β-decay signal.

As part of a systematic investigation of the Ru isotopes, we have initiated a program of Coulomb-excitation studies to complement the existing detailed results for ^{104}Ru. The aims of the measurements are to provide precise values of the shape invariant quantities $\langle Q^2 \rangle$ and $\langle Q^3 \cos 3\delta \rangle$ for the ground states and 0_2^+ states across the stable Ru isotopes. Herein, we report the results of Coulomb excitation of ^{102}Ru performed with beams of ^{12}C and ^{16}O and analyzed using a magnetic spectrograph. The use of the relatively light ions ^{12}C and ^{16}O to excite states in ^{102}Ru assures that the reaction process is dominated by a single-step excitation directly from the ground state. Used extensively in early Coulomb-excitation studies, measurements with magnetic spectrographs were superseded by those with γ-ray spectrometers with Ge detectors that provide a 20-fold (or more) increase in peak resolution; to the authors' knowledge, the most recent published report of the use of a magnetic spectrograph for Coulomb excitation was the measurement of the $E3$ excitations in the Hg isotopes by Lim *et al.* [30] in 1991. We hope that the present work illuminates this long-dormant technique's usefulness in Coulomb-excitation studies.

II. EXPERIMENTAL DETAILS AND RESULTS

The measurements were performed at the Maier Leibnitz Laboratory of the Technische Universität and the Ludwig-Maximilians Universität München. Beams of ^{12}C ions with energies of 53 MeV (hereafter labeled *expt1*), 45 MeV (*expt2*), and currents up to 200 pnA, and ^{16}O ions with energies of 56 MeV (*expt3*) and currents up to 180 pnA bombarded a target of ^{102}Ru with a thickness of $\approx$40 µg/cm^2 on a carbon backing 10 µg/cm^2 thick. The ions scattered from the target were momentum analyzed with a Q3D magnetic spectrograph, and their positions on the focal plane were recorded with detectors that used proportional counters for position and energy loss. The detector used in *expt1* was a 1-m-long Frisch-grid ionization chamber to measure the total energy, which had four ΔE sections with two position-sensitive proportional counters inserted [31]. The detector for *expt2* and *expt3* used a single-wire proportional counter to measure ΔE, and the residual energy was measured with 96 Si detectors, each of which was 10 mm wide and 30 mm high with a 1 mm gap between adjacent detectors resulting in an 11 mm pitch, and 0.4 mm thickness (a prototype is described in Ref. [32]). The data from *expt1* exhibited the lowest background and greatest resolution. Data were recorded at spectrograph angles of 20°, 25°, 30°, 35°, and 41° degrees (*expt1*), 30°, 45°, 50°, and 55° degrees (*expt2*), and 45°, 53°, and 60° degrees (*expt3*). This selection of angles spanned both the "safe" and
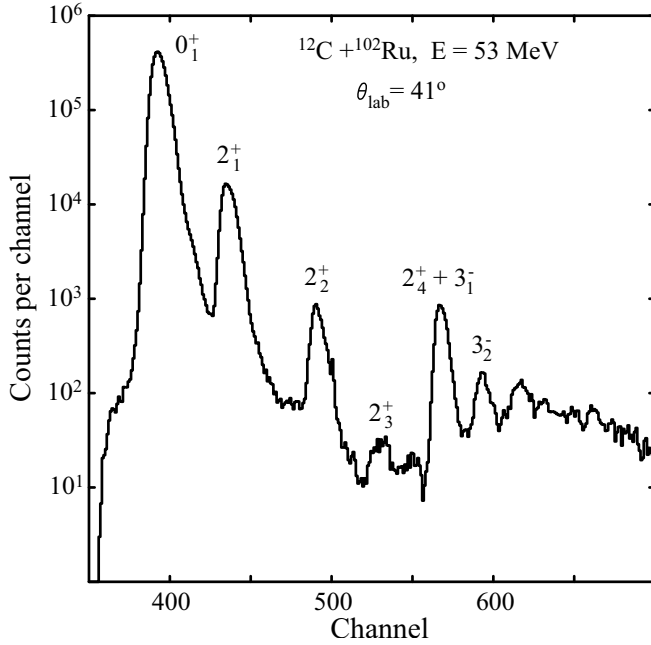
FIG. 2. Spectrum observed at 41° degrees resulting from the scattering of ^{12}C ions at 53 MeV from a ^{102}Ru target. The peaks are labeled with the angular momentum and parity of the corresponding state in ^{102}Ru.

"unsafe" regimes (described below) for the beam energies used.

The acceptance of the scattered ions from the target chamber to the magnet chamber was controlled with an aperture with adjustable slits, and the settings employed were such that the solid angle subtended was ≈10 msr, with ≈ ± 4° in the vertical direction and ≈ ± 2° in the horizontal. The vertical focusing of the spectrograph, and the dimensions of the detectors, ensured that all ions that satisfied the $B\rho$ selection would impinge on the detector. The magnetic field of the spectrograph was adjusted such that the elastically scattered ions, those with the greatest magnetic rigidity, impinged on the detector near its one end. With the magnetic field adjusted in this way, the detector length enabled acceptance of scattered ions from states up to an excitation energy above 4 MeV in the ^{102}Ru target nucleus. Shown in Fig. 2 is the ^{12}C ion spectrum obtained from *expt1* with a spectrograph angle of 41°, which demonstrates the excellent resolution, ≈100-keV full-width at half maximum, obtained in the present measurements.

The usual condition applied to ensure purely electromagnetic interactions is that the distance of closest approach of the nuclear surfaces s should be $\geqslant 5$ fm. However, as has been previously investigated [35–43], this does not apply for relatively light ions such as ^{12}C and ^{16}O, for which nuclear effects have been observed at distances beyond 5 fm. We therefore followed, in the initial analysis, a conservative approach of adopting $s = 6.5$ fm as the minimum separation distance. Using

$$d_{\min} = 1.25\left(A_p^{1/3} + A_t^{1/3}\right) + 6.5 \text{ fm}, \tag{1}$$

the relationship between the angle and beam energy

$$E_p = \frac{1.44}{2}\left(\frac{A_p + A_t}{A_t}\right)\frac{Z_p Z_t}{d_{\min}}\left(1 + \frac{1}{\sin(\theta_{\text{c.m.}}/2)}\right) \text{ MeV} \tag{2}$$

was solved to provide the maximum center-of-mass scattering angle, $\theta_{\text{c.m.}}$, that was adopted in the analysis for the given beam energy E_p. In the subsequent analysis, the 6.5 fm separation criterion was reassessed as will be discussed in the following.

The population P_i of the ith excited state was extracted by taking the ratio of the area of a peak A_i in the spectrum to the sum of the area of the ground-state and 2_1^+-state peaks:

$$P_i = \frac{A_i}{A_{gs} + A_{2_1^+}}, \tag{3}$$

i.e., we use the approximation that $(A_{gs} + A_{2_1^+}) \simeq \sum A_i$ since the populations of states above the 2_1^+ state are typically below 0.1%. Furthermore, this approximation guaranteed consistency across all angles and experiments since peaks due to higher-lying states were unobserved in some spectra, and eliminated unknown background contributions. As the populations are determined from ratios of peak areas within a single spectrum, many of the systematic effects, such as target thickness and uniformity, data-acquisition dead times, beam fluctuations, etc., are in common. However, as can be seen in Fig. 2, the peak shapes involve rather long "tails" on which peaks due to excited states may be located. The peak-shape model included an exponential tail, and consistent fits of the 2_1^+ and 2_2^+ peak areas were only obtained fitting the ground-state, 2_1^+, and 2_2^+ peaks as an ensemble. For the higher-lying states, fits were performed taking a smooth polynomial background. In addition to the statistical uncertainty, systematic uncertainties of 3% on the ground-state peak area, and 5% on excited-state peak areas (a larger value was taken to account for uncertainties in the modeling of the exponential tail), were adopted and added in quadrature. The populations extracted from the spectra are listed in Table I.

The state populations were fit using the GOSIA code [44]. Figure 3 displays the coupling scheme used in the present calculations. The arrows with numerical values, namely the $2_1^+ \rightarrow 4_1^+$ and $2_1^+ \rightarrow 2_2^+$ transitions along with the diagonal matrix element of the 2_1^+ state, correspond to the matrix elements that were held fixed in the analysis at the values given. For each of the remaining transitions in Fig. 3, the corresponding matrix element was varied, and the χ^2 value using the uncertainty-weighted square of the difference between the observed and predicted population was minimized. The value of the $\langle 2_2^+ \|E2\| 2_1^+ \rangle$ matrix element in the calculations uses the evaluated branching and multipole mixing ratio data listed in Ref. [33], and was set relative to the fit $B(E2; 0_1^+ \rightarrow 2_2^+)$ value determined in the present work.

Panels on the right-hand side of Fig. 4 show the populations of the 2_1^+, 2_2^+, 3_1^-, and 3_2^- states, the latter spin-parity assigned firmly in the present work as described below, obtained in *expt1* as a function of the ^{12}C scattering angle. Also shown are the populations predicted using GOSIA along with the $\pm 1\sigma$ uncertainties obtained from the matrix elements that resulted in a $\chi^2_{\min} + 1$ value, shown on the left-hand side of Fig. 4.

TABLE I. Populations expressed as $10^3 \times P_i$ derived using Eq. (3) from the measurements with ^{12}C at 53 MeV (*expt1*) and 45 MeV (*expt2*), and ^{16}O at 56 MeV (*expt3*). The uncertainties on the populations include a 3% systematic uncertainty for the area of the elastic peak, and a 5% systematic uncertainty for the excited-state peaks that have been added in quadrature.

E_{ex} (keV)	I_i^π	*expt1*				
		20°	25°	30°	35°	41°
475.1	2_1^+	4.2(10)	6.9(5)	12.1(8)	24.1(14)	37.5(23)
1103.0 1106.4	2_2^+ 4_1^+	0.096(18)	0.316(23)	0.515(33)	0.78(5)	1.62(11)
1580.6[a]	2_3^+					0.029(6)
2036.7 2043.4	2_4^+ 3_1^-	0.036(10)	0.071(7)	0.190(13)	0.478(32)	1.54(9)
2367.3[b]	3_2^-		0.010(5)	0.028(7)	0.088(18)	0.262(15)
		expt2				
		30°	45°	50°	55°	
475.1	2_1^+	7.9(7)	26.6(16)	42.8(26)	62.9(37)	
1103.0 1106.4	2_2^+ 4_1^+	0.49(15)	1.12(9)	1.52(19)	2.48(21)	
		expt3				
		45°	53°	60°		
475.1	2_1^+	35.2(22)	57.2(35)	76.1(45)		
1103.0 1106.4	2_2^+ 4_1^+	1.58(13)	2.94(22)	4.96(48)		
2036.7 2043.4	2_4^+ 3_1^-	0.397(27)	0.70(11)			

[a]Peak observed at 41° in *expt1* only.
[b]Peak observable above background in *expt1* only.

The largest angles used in the three experiments corresponded to separations between the nuclear surfaces of $s = 5.7$ fm (*expt1*), 5.4 fm (*expt2*), and 5.6 fm (*expt3*), and the initial χ^2 analysis omitted these data. The predicted populations at the largest measured angles were compared with the observed populations, as shown in Fig. 5 for the 2_1^+ and 2_2^+ states. As can be seen, a deviation in the 2_1^+ population ratio is observed for the 5.4 fm separation only. We therefore concluded that the 6.5 fm separation condition could be relaxed for $E2$ excitations, and we included in the analysis the data obtained at the largest angles in *expt1* and *expt3*. For $E3$ excitations, it is obvious from Fig. 4 that at 41° the populations of the 3^- states greatly exceed the GOSIA predictions, and we continue to enforce the 6.5 fm separation criteria. Moreover, the strong population of the 2367-keV state, previously assigned as possessing spin-parity of $(3^-, 4^+)$ [33], in one-step Coulomb excitation from the 0^+ ground state, combined with its observed significant enhancement for $s < 6.5$ fm, provides evidence for the 3^- spin-parity assignment of this level.

To explore further the possible role of nuclear effects contributing to the population of 2^+ states in the scattering of ^{12}C from ^{102}Ru, calculations with the FRESCO code [45] were performed. Several available optical-model parameter (OMP)

sets [46–48] for ^{12}C were evaluated by comparing calculated cross sections with elastic- and inelastic-scattering data for the ^{12}C + ^{100}Mo reaction at 48 MeV [46]. Of the parameter sets tested, those of Gan *et al.* [47], that result from a global fit of ^{12}C reaction data, were judged to give the best reproduction of the Mo data [46]. While the aim of the calculations was to test the magnitude of the nuclear effects in our Coulomb-excitation reaction rather than perform detailed fits, small adjustments were made in the OMPs nonetheless in order to improve the quality of the fit to the Mo target data—namely, the real well diffuseness was increased by 0.05 fm, and the depth of the imaginary well increased by 30 MeV. The optical model parameters, given in Table II, were then used in the calculation of the population of the 2_1^+ state in ^{102}Ru with the nuclear deformation parameters calculated from the $B(E2)$ values determined from the GOSIA analysis. The results of the FRESCO calculations, for the scenarios of Coulomb-only and Coulomb + nuclear interactions, are shown in Fig. 6. The inclusion of the nuclear interaction induces oscillatory deviations from the values calculated with the Coulomb interaction only. The curves resulting from the full calculation generally pass within the uncertainties of the experimental data, with the only significant outlier being the data point at the largest
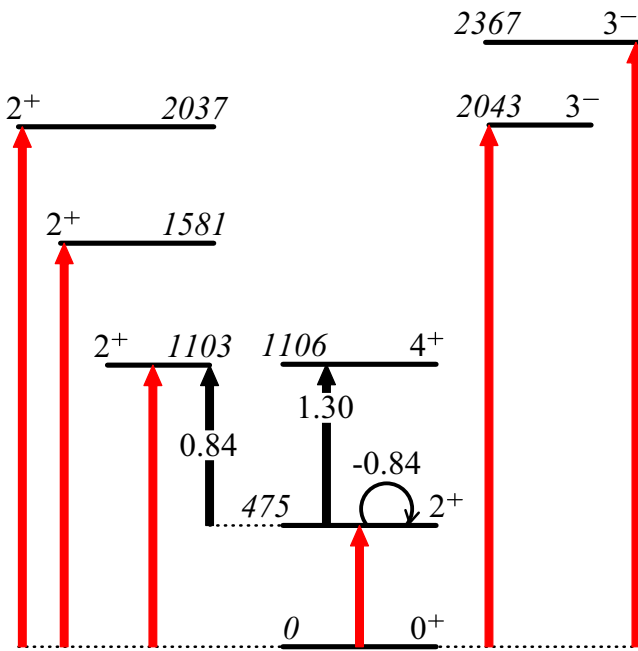
FIG. 3. Coupling scheme used in the GOSIA calculations. The black arrows represent matrix elements that were held fixed in the analysis at the values given by their labels (in *e* b), which are taken from Ref. [33]; that for the $2_1^+ \rightarrow 2_2^+$ transition was fixed using the present value for the $0_1^+ \rightarrow 2_2^+$ transition and sign as determined in Ref. [34].

angle from the 45-MeV data set. Furthermore, while the experimental data were taken at angles that fall near the crossing points of the curves, the magnitudes of the differences are also within the experimental uncertainties on the populations, indicating that ignoring the nuclear contribution does not substantially bias the extracted results. This provides confidence that accurate determination of an $E2$ matrix element could be achieved by reproducing, using GOSIA, an observed population at a single angle—a procedure which will be used below.

The coupling scheme displayed in Fig. 3 includes some selected two-step processes for completeness, but the effects were mostly small. For example, for the *expt1* data, the $\langle 2_2^+ \| E2 \| 0_1^+ \rangle$ matrix element changes from 0.1588(33) *e* b (including the $2_1^+ \rightarrow 2_2^+$ coupling) to 0.1615(32) *e* b (without the $2_1^+ \rightarrow 2_2^+$ coupling), or 1.7%—well within the uncertainty. The population of the 4_1^+ state, on the other hand, had to be taken into account since the 4_1^+ state was unresolved from the 2_2^+ state. The predicted populations of the 4_1^+ level, using the known [33] $B(E2; 4_1^+ \rightarrow 2_1^+) = 66(11)$ W.u., are significant fractions of the populations of the 2_2^+ level, especially at the higher angles. Rather than performing a two-dimensional χ^2 analysis such as that performed for the $3_1^-/2_4^+$ doublet described below, we used the calculated 4_1^+ populations and subtracted these contributions to arrive at the corrected populations for the 2_2^+ state. The corrected and uncorrected populations are shown in Fig. 4(d), and the uncertainties on the former include the contribution of the uncertainty on the $B(E2; 4_1^+ \rightarrow 2_1^+)$ value. The values extracted from the three

measurements are listed in Table III and are in nearly perfect agreement.

A peak attributed to the 2_3^+ state at 1581 keV was observed, as shown in Fig. 2, in *expt1* at 41° only. The extracted population was $2.9(6) \times 10^{-5}$, which would correspond to a $\langle 2_3^+ \| E2 \| 0_1^+ \rangle$ matrix element of 0.0274(29) *e* b, or $B(E2; 2_3^+ \rightarrow 0_1^+) = 0.053(11)$ W.u. This value coincides with the upper limit given by Börner *et al.* [1]. Taking into account the contribution from the nuclear interaction for the population of the 2_3^+ level, using the FRESCO calculations described above, would require a reduction of the matrix element by approximately 8%, well within the 11% uncertainty of the measurement. Since we cannot extract the 2_3^+ population for other angles, we are unable to judge the reasonableness of the calculated nuclear contribution, and we thus report the value determined from the GOSIA analysis, i.e., assuming a pure electromagnetic interaction only, for consistency with the results for other states. The reliance on a single datum also implies that we cannot perform a consistency check of the population as a function of the scattering angle, contrary to the results for other levels. However, there are no known impurities in the target that would contribute to the 2_3^+ peak area.

Another unresolved doublet occurs at the level of the 3_1^- state at 2043 keV with the 2_4^+ state at 2037 keV. No information was available to estimate the population of the 2_4^+ level, and two approaches were taken. In the first, the assumption was made that population of the 2_4^+ state was negligible, and thus the population data were fit using only the $0_1^+ \rightarrow 3_1^-$ excitation, as shown in Fig. 4. As can be seen, assuming only the $E3$ excitation yields an excellent reproduction of the doublet population for the four lowest angles. In the second approach, a two-dimensional χ^2 surface was constructed by varying both the $\langle 2_4^+ \| E2 \| 0_1^+ \rangle$ and $\langle 3_1^- \| E3 \| 0_1^+ \rangle$ matrix elements. The data from a single experiment were insufficient to constrain the values in any reasonable way, and thus a simultaneous analysis of the data from both *expt1* and *expt3* was performed (the data from *expt2* unfortunately had a higher background level in this region of the spectrum, and were disregarded in this analysis). Figure 7 displays the results of the second analysis; for clarity, the χ^2 values are limited to the region with $\chi_{min}^2 + 1$. The values of the matrix elements that resulted in the minimum χ^2 value, and the uncertainties evaluated for the extrema points for $\chi^2 + 1$, are given in Table III.

Using the spectroscopic data as given in Ref. [33] for the 2_4^+ level, the results of the 2*D* fitting procedure leads to very large $B(E2)$ values for the $2_4^+ \rightarrow 2_1^+$ ($\simeq 9$ W.u.), $2_4^+ \rightarrow 4_1^+$ ($\simeq 40$ W.u.), and the $2_4^+ \rightarrow 2_3^+$ ($\simeq 4.6 \times 10^3$ W.u. assuming pure $E2$) transitions with uncertainties of nearly 100%. These values would be very difficult to understand. A further limit on the contribution of the $E2$ matrix element can be given by consideration of the over-population recorded at the highest angle, as shown in Fig. 4, for the 3^- states in contrast to the behavior of the 2^+ levels that display no overpopulation. The enhancement for the 3_2^- level is found using the observed population and subtracting the GOSIA prediction at 41°, and amounts to 59(19)% relative to the predicted GOSIA population. This over-population of the 3_2^- level is ascribed
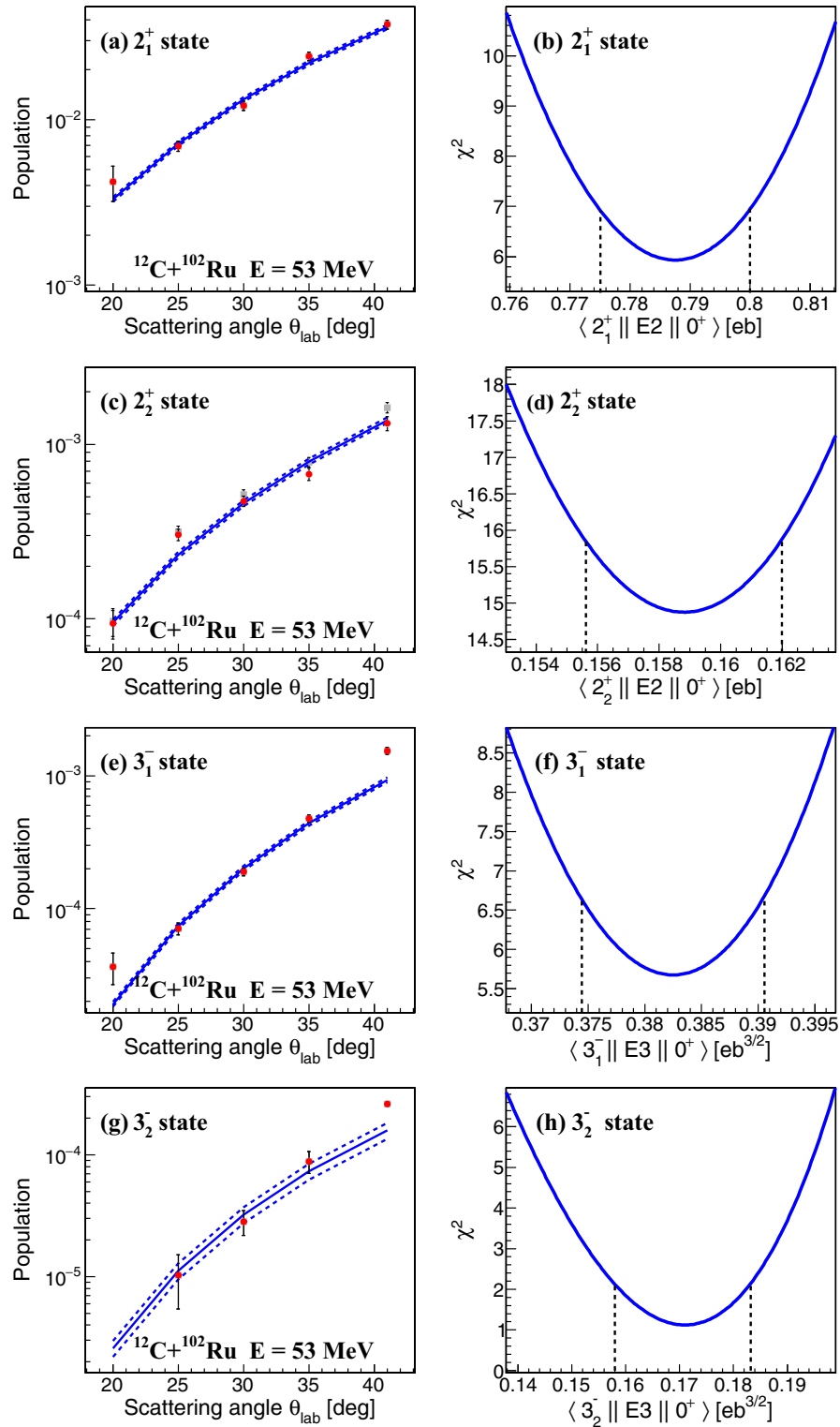
FIG. 4. Results for (a), (b) the 2_1^+, (c), (d) 2_2^+, (e), (f) 3_1^-, and (g), (h) 3_2^- states in ^{102}Ru obtained from the Coulomb-excitation reaction with 53-MeV ^{12}C ions. The experimental populations are shown in panels (a), (c), (e), and (g) as a function of the ^{12}C scattering angle. The solid curves are the calculated populations using the matrix elements determined from the minimum of the χ^2 value as a function of the $\langle I^\pi \| E\lambda \| 0_1^+\rangle$ matrix element shown in panels (b), (d), (f), and (h), while the dashed curves are values obtained including the $\pm 1\sigma$ uncertainties. Shown in panel (c) are the populations for the unresolved $2_2^+/4_1^+$ doublet (gray squares) and the populations for the 2_2^+ state obtained by subtracting the calculated populations of the 4_1^+ state using the $B(E2; 4_1^+ \rightarrow 2_1^+)$ given in Ref. [33] (red circles). Panels (e) and (f) display the population and fit to the $2_4^+/3_1^-$ doublet, assuming only the $E3$ excitation. For 2^+ states, fits are performed to five data points, and for the 3_1^-, 3_2^- states to four and three points, respectively (with the point at $41°$ excluded, as described in the text).
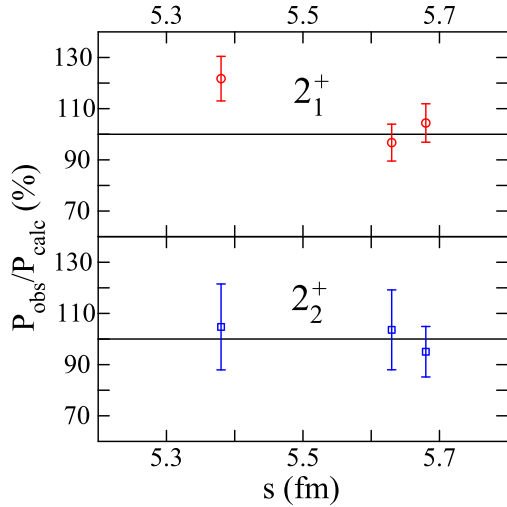
FIG. 5. Ratio of the observed population to the predicted population for the 2_1^+ and 2_2^+ states in ^{102}Ru as a function of the separation between the nuclear surfaces calculated from Eqs. (1) and (2). The predicted populations are results of fits performed using data obeying the condition $s \geqslant 6.5$ fm.

to the nuclear $E3$ contribution. Since the excitation energies of the 3_2^- and 3_1^- states are very similar, we expect a very similar enhancement factor for the latter. This is realized, with the $3_1^-/2_4^+$ doublet possessing a 64(10)% enhancement. The difference in these two results, $-5(21)\%$, gives a 1σ upper limit to the $E2$ contribution to the population of the doublet of 16%, translating to a lower limit for the $E3$ matrix element to be >0.35 $e\,\mathrm{b}^{3/2}$. This limit would exclude the entire region in the χ^2 distribution contained within $\chi_{\min}^2 + 1$ limit. Thus, we strongly favor the results for the $E3$ matrix element extracted without the contribution of the $E2$ excitation for the doublet. (Note that the data for the decay of the 2037-keV 2_4^+ state have very large uncertainties that hamper making structural assignments.) Taking a weighted average of the results for *expt1* and *expt3*, the result is $\langle 3_1^- \| E3 \| 0_1^+ \rangle = 0.369 \pm 0.018_{\mathrm{stat}}$ $e\,\mathrm{b}^{3/2}$, where the uncertainty is the standard deviation of the mean, yielding $B(E3; 3_1^- \to 0_1^+) = 31.5 \pm 3.1_{\mathrm{stat}} \pm 1.6_{\mathrm{sys}}$ W.u., or 31.5 ± 3.5 W.u. adding the statistical and systematic uncertainties in quadrature.

Presented in Fig. 8 is a summary of the matrix elements for the 2_1^+ and 2_2^+ excitations extracted from the three experiments, also showing the evaluated values from Ref. [33].

TABLE II. Optical model parameters (OMPs) for the FRESCO calculations, described in the text, for the reaction ^{12}C $+ ^{102}$Ru at 53-MeV beam energy. The potential used a volume Woods-Saxon form with real and imaginary components with depths V and W, a common radius r, and diffuseness parameters a_R and a_W as described in Ref. [47]. Compared with the values from computed expressions given in Ref. [47], a_R was increased by 0.05 fm, and W increased by 30 MeV.

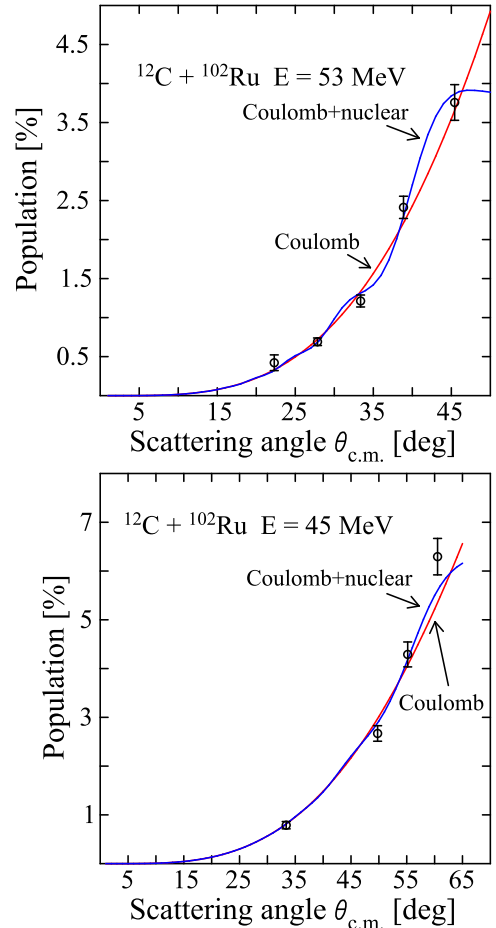| V (MeV)	r (fm)	a_R (fm)	W (MeV)	a_W (fm)
268.7	1.071	0.627	157.6	0.577

FIG. 6. Populations of the 2_1^+ state in ^{102}Ru using ^{12}C beams at 53 MeV (top panel) and 45 MeV (bottom). The data points are from the present measurements, and the curves are the calculated populations using the FRESCO code [45] that take into account the Coulomb interaction only (red line), and the Coulomb + nuclear interaction using the optical model parameters described in the text (blue line).

The ^{12}C data at the two beam energies are in excellent agreement. The $\langle 2_1^+ \| E2 \| 0_1^+ \rangle$ matrix element from the ^{16}O data is approximately 6% smaller than those resulting from the ^{12}C measurements and is lower than the evaluated matrix element [33] by approximately 2.2σ. Performing a weighted average, with the statistical uncertainties only, of the currently obtained values of matrix elements, we arrive at a value of $B(E2; 2_1^+ \to 0_1^+) = 41.5 \pm 0.9_{\mathrm{stat}} \pm 2.1_{\mathrm{sys}}$ W.u. or 41.5 ± 2.3 W.u. The matrix elements for the 2_2^+ state are in excellent agreement for the three measurements, within uncertainty and to within 4%, but are approximately 20% greater than the evaluated matrix element [33]. Our final result is $B(E2; 2_2^+ \to 0_1^+) = 1.75 \pm 0.06_{\mathrm{stat}} \pm 0.09_{\mathrm{sys}}$ W.u. or 1.75 ± 0.11 W.u.

The local systematics of the $B(E3; 3_1^- \to 0_1^+)$ values are shown in Fig. 9. No new results for $B(E3)$ values in Mo, Ru, or Pd nuclei have occurred since the evaluation of Kibédi and Spear [49] with the exception of ^{100}Mo, where a recent Coulomb-excitation study found significantly greater $E3$

TABLE III. Values of the matrix elements, in units of eb for $E2$ transitions, and $eb^{3/2}$ for $E3$ transitions, extracted from the present experimental data. For the $3_1^-/2_4^+$ unresolved doublet, two analyses are reported: one fitting the population with an $E3$ contribution only, and the second using a combined analysis of the *expt1* and *expt3* data with $E2$ and $E3$ contributions. The 1σ uncertainties, extracted from the $\chi^2 + 1$ analysis, are given on the last digit, and do not include an estimated 2.5% systematic uncertainty arising from the assumptions used in GOSIA [44]. The rightmost column lists the previously known values from the references indicated.

| E_{ex} (keV) | I_i^π | $\langle I^\pi \Vert E\lambda \Vert 0_1^+ \rangle$ | | | |
		expt1	*expt2*	*expt3*	Lit.
475.1	2_1^+	0.788(13)	$0.777^{+0.015}_{-0.016}$	0.733(13)	0.795(6)[a]
1103.0	2_2^+	0.1588(33)	0.154(7)	0.155(8)	0.127(8)[a]
1580.6[b]	2_3^+	0.0274(29)			<0.027[c]
2043.4	3_1^-	0.381(8)[d]		0.347(11)[d]	0.255(25)[e]
2367.3[f]	3_2^-	$0.171^{+0.012}_{-0.013}$			
			expt1 + expt3		
2036.7	2_4^+		$0.11^{+0.03}_{-0.05}$[g]		
2043.4	3_1^-		$0.28^{+0.06}_{-0.08}$[g]		0.255(25)[e]

[a]Reference [33].
[b]Peak observed at $41°$ in *expt1* only.
[c]Reference [1].
[d]Fit performed assuming $0_1^+ \rightarrow 3_1^-$ excitation only.
[e]Reference [49].
[f]Peak observable above background in *expt1* only.
[g]Fit performed using $0_1^+ \rightarrow 3_1^-$ and $0_1^+ \rightarrow 2_4^+$ excitations.

strength [24]. Using the favored one-parameter fit for the $2_4^+/3_1^-$ doublet, the present result for ^{102}Ru is significantly greater than previous values, but more consistent with the $E3$ strength observed in the Mo isotopes. These new results for ^{100}Mo [24] and ^{102}Ru indicate that the $E3$ strength in this region should be reexamined.

III. DISCUSSION

We compare the results with calculations performed using the symmetry-conserving configuration-mixing (SCCM) method employing the Gogny-D1S energy-density functional as the interaction [53]. In this method, the nuclear wave functions are defined as linear combinations of
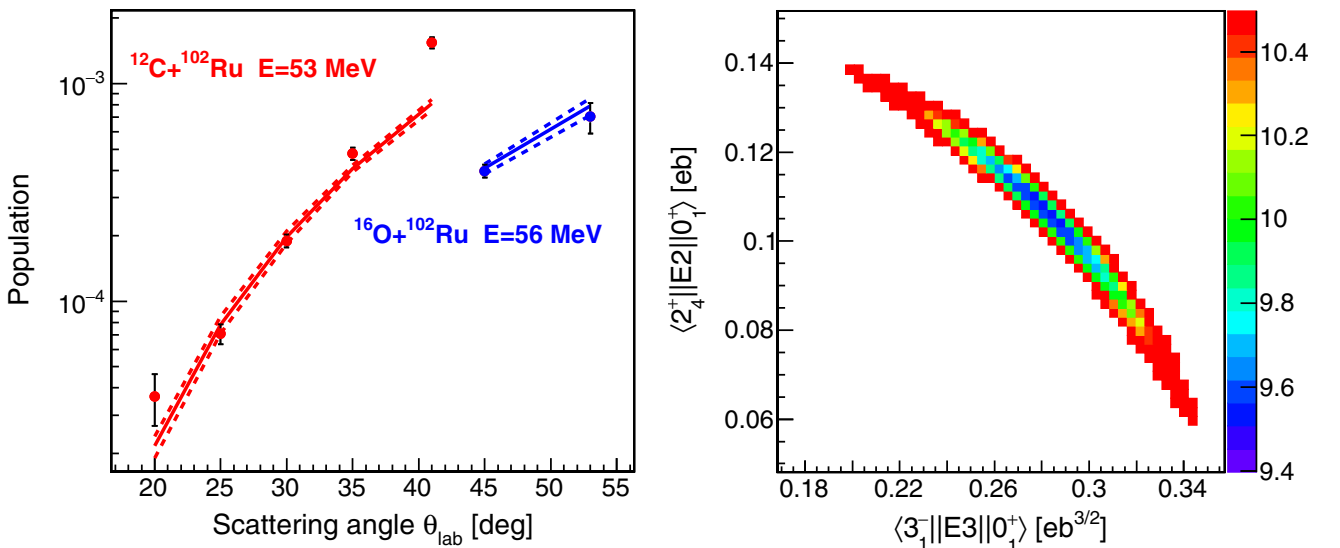

FIG. 7. Analysis of the data for the unresolved $2_4^+/3_1^-$ doublet. The right panel displays the χ^2 value obtained as a function of both the $\langle 2_4^+ \Vert E2 \Vert 0_1^+ \rangle$ and $\langle 3_1^- \Vert E3 \Vert 0_1^+ \rangle$ matrix elements. The population data obeying the $s \geqslant 6.5$ fm separation criteria from *expt1* and *expt3* were used, and the resulting fit using the matrix elements from the $\chi^2_{\min}$ point is shown on the left.
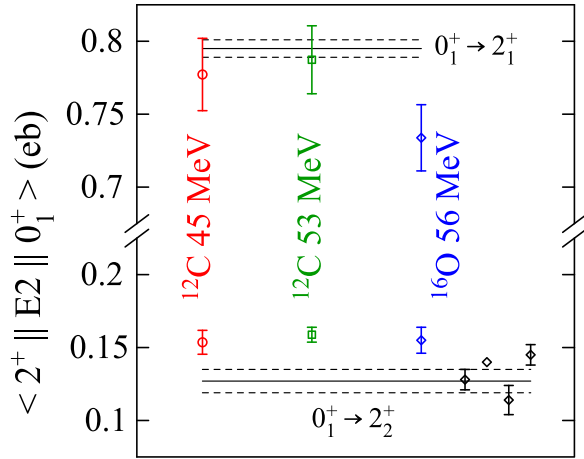
FIG. 8. Summary of the matrix elements for the $0_1^+ \rightarrow 2_1^+$ and $0_1^+ \rightarrow 2_2^+$ transitions (colored points) with labels indicating the beam used to perform the measurement. The solid lines are the evaluated values from Ref. [33], with the dashed lines indicating their $\pm 1\sigma$ uncertainties. Also shown are the available data for the $0_1^+ \rightarrow 2_2^+$ transition from Refs. [34,50–52] (black points). The data point without an uncertainty, from Ref. [34], resulted from an analysis that concluded a constructive interference for the population of the 2_2^+ level.

particle-number and angular-momentum-projected Hartree-Fock-Bogoliubov (HFB) states with different quadrupole deformations parametrized by (β_2, γ). Such HFB wave functions are obtained by using the particle-number variation-after-projection method (PN-VAP). The present implementation of the SCCM method is particularly suitable to describe qualitatively collective aspects of the nuclear structure from a microscopic point of view. Notably, shape evolution and
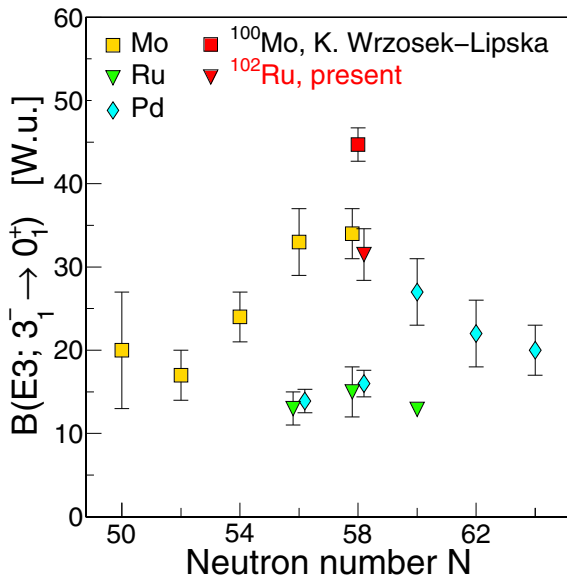

FIG. 9. Values of $B(E3; 3_1^- \rightarrow 0_1^+)$ observed in the Mo (yellow squares), Ru (green triangles), and Pd (blue diamonds) isotopes from the evaluation of Ref. [49], presented together with the new result for ^{100}Mo [24] (red square, labeled ^{100}Mo) and the present result (red triangle, labeled ^{102}Ru).
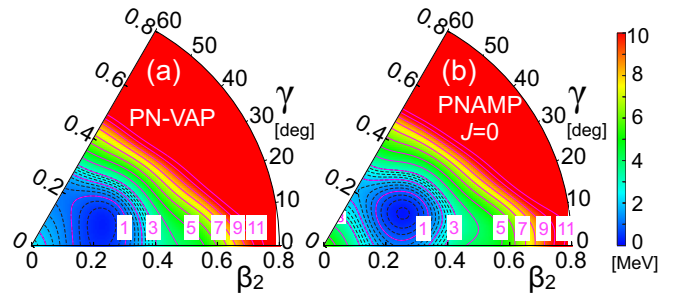

FIG. 10. (a) Particle-number variation-after-projection (PN-VAP) and (b) particle-number and angular-momentum projection (PNAMP, $J = 0$) energies in the (β_2, γ) plane for ^{102}Ru calculated with the Gogny-D1S interaction.

coexistence, and the mixing of shapes, can be studied within this framework. However, neither parity nor time-reversal symmetries are broken. As a consequence, negative-parity states cannot be computed and, additionally, the excited states (including noncollective states) are not as well explored as the ground state of the nucleus [54,55].

We can obtain a first global picture of the collective nature of the nucleus by analyzing the mean-field energy (in our case, the PN-VAP energy) as a function of the quadrupole deformation, i.e., the PES. In Fig. 10(a) we observe that the PN-VAP energy displays only one minimum at $(\beta_2, \gamma) = (0.22, 0°)$ although the PES is rather flat in a range of $\beta_2 \in [0.0, 0.3]$. Beyond-mean-field correlations can modify this picture as it is shown in Fig. 10(b) where the particle-number and angular-momentum-projected ($J = 0$) energy is plotted. Here we see that the axial minimum has been shifted towards a well-defined triaxial minimum at $(0.25, 20°)$. Nevertheless, the final results (excitation energies, electromagnetic properties, transition probabilities, and collective wave functions) are obtained after performing the configuration (shape) mixing.

The collective wave functions resulting from the calculations are displayed in Fig. 11. The 0_1^+ and 0_2^+ states are predicted to have a triaxial shape, with the ground-state having $(\beta_2, \gamma) = (0.25, 20°)$, and the 0_2^+ state possessing a very broad distribution in the (β_2, γ) plane. The 0_3^+ state displays a high degree of shape mixing, with substantial contributions from both prolate, with $\beta_2 \simeq 0.35$, and oblate, with $\beta_2 \simeq 0.2$, shapes. The predicted ground-state shape is consistent with the results of recent calculations with the relativistic Hartree-Bogoliubov formalism [16] using the density-dependent ME2 [56] and PC1 [57] parametrizations that predict minima in the PES of $(\beta_2, \gamma) = (0.25, 15°)$ and $(0.25, 17°)$, respectively. Nearly identical results [17] were found using the covariant density function theory with the PC-PK1 interaction [58] that yields a minimum at $(0.25, 19°)$. The calculations using a self-consistent mean-field using the Gogny-D1M interaction predict that ^{102}Ru possesses some γ softness but with a prolate minimum at $\beta_2 \simeq 0.2$ [15].

Shown in Fig. 12 is a comparison of the experimental data for low-lying levels in ^{102}Ru and the results of the SCCM calculations. It can be seen that the degree of quadrupole collectivity is predicted to be greater than that observed, with the $B(E2)$ values in the ground-state band approximately 50%
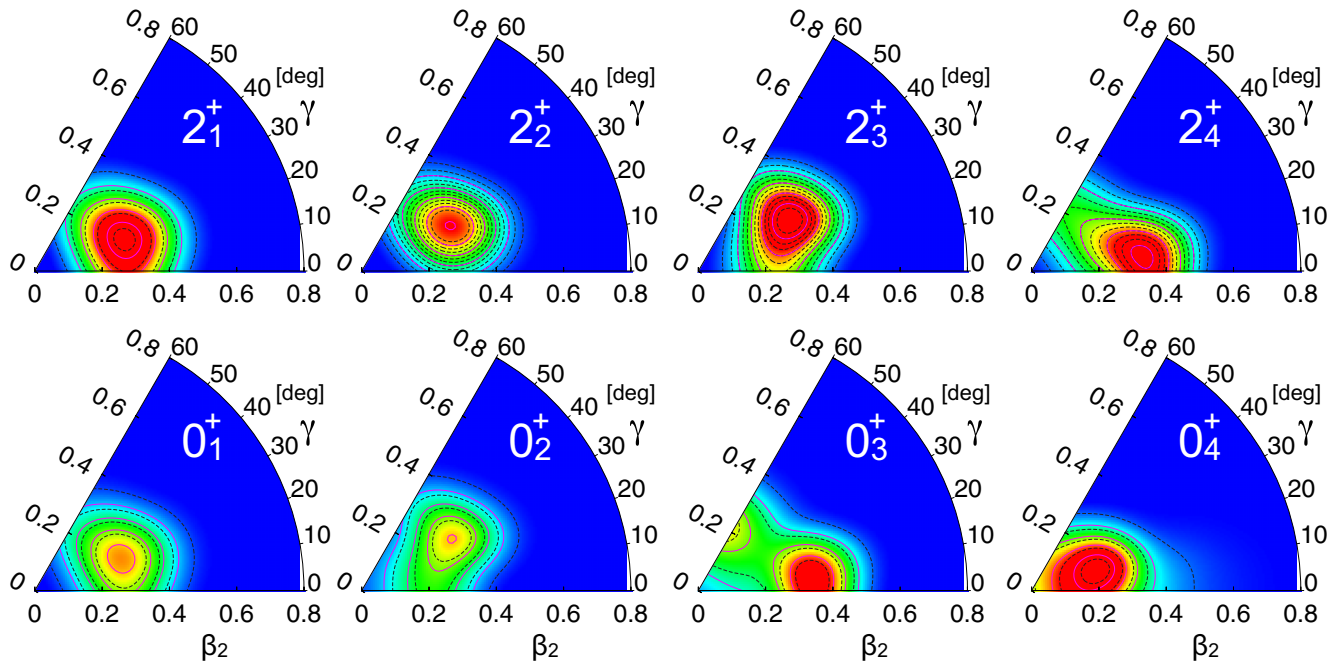
FIG. 11. Collective wave functions in the (β_2, γ) plane for the first four 0^+ and 2^+ states in ^{102}Ru.

larger than the experimental values. This is an indication of the overestimation of the deformation by the SCCM method in this case. Another hint of this limitation is the almost perfect description of the 2_1^+ excitation energy with a SCCM method that does not include time-reversal symmetry-breaking states [55]. The most plausible explanation for this discrepancy is the use of a beyond-mean-field method with an underlying interaction that was fit to reproduce experimental ground-state properties at the mean-field level. The angular-momentum restoration is very effective to include correlation energies for deformed configurations. Therefore, these beyond-mean-field effects can produce an excess of deformation for nearly spherical or soft nuclei. Improving the parametrization of the underlying interaction should be the best way to correct this overestimation. The transition rates for the decay from the γ-bandhead are approximately 80% of the theoretical values.
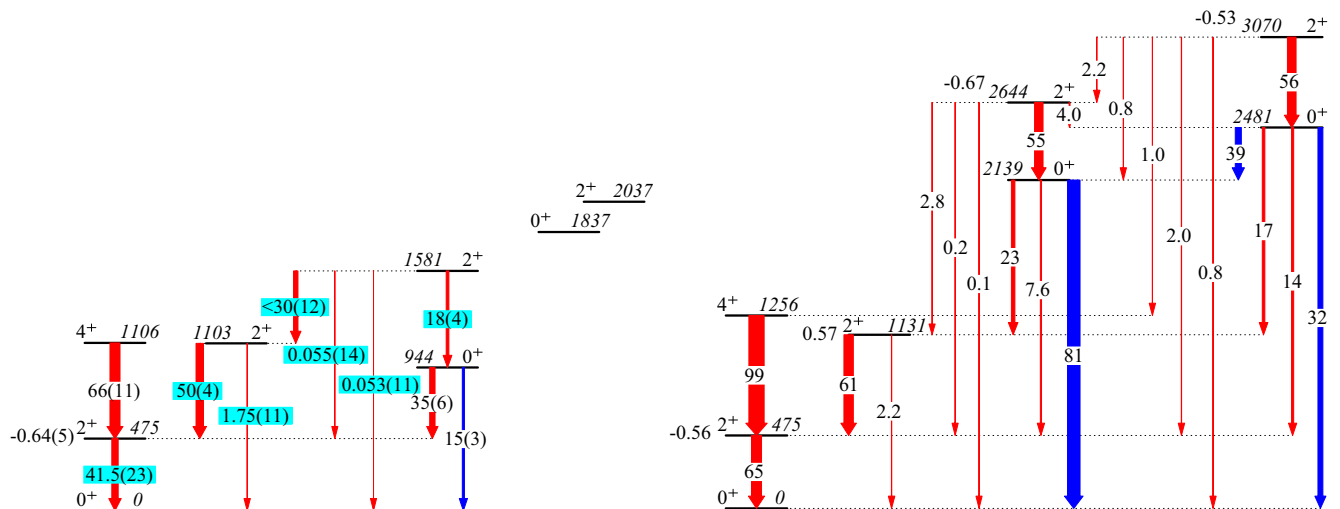

FIG. 12. Data for low-lying levels in ^{102}Ru. The level scheme on the left shows the experimental data; transitions in red are labeled with their $B(E2)$ values in W.u., those in blue are $1000\rho^2(E0)$ values, and the uncertainties are given in parentheses. The values within the colored boxes are calculated using results from the present measurements, otherwise they are taken from Refs. [33,59]. The spectroscopic quadrupole moment in e b, where known, is written to the left of the level. For the 1581-keV 2_3^+ level, the spectroscopic data are taken from Ref. [20], and the upper limit reflects the unknown mixing ratio. The 2_4^+ state at 2037 keV is not assigned as the band member of the 0_3^+ state at 1837 keV, but it is the highest energy, firmly assigned 2^+ level in ^{102}Ru. The level scheme on the right is the result of the SCCM calculations and uses the same labeling convention.

The 0_2^+ state is predicted to be located far higher in excitation energy than observed, with the $B(E2; 0_2^+ \to 2_1^+)$ value a factor of five smaller than the observed value, and further a moderate $B(E2; 0_2^+ \to 2_2^+)$ value predicted. Most notably, the predicted $\rho^2(E0; 0_2^+ \to 0_1^+)$ is nearly a factor of six larger than the experimental value, indicating a higher degree of shape mixing in the calculations compared with the experimental data.

The Kumar-Cline sum rules [60] can be used to extract the rotationally invariant $E2$ moments for the 0^+ states from

$$\frac{1}{\sqrt{5}}Q^2 = \sum_i \langle 0\|E2\|2_i\rangle\langle 2_i\|E2\|0\rangle \begin{Bmatrix} 2 & 2 & 0 \\ 0 & 0 & 2 \end{Bmatrix}, \quad (4)$$

where {} is a $6j$ symbol. While the sum extends over the complete set of 2^+ states, it generally is determined by a few key matrix elements. The Q^2 invariant can be related to the β_2 shape parameter within the axially symmetric rotational model via

$$Q^2 = q_0^2|\beta_2|^2, \quad (5)$$

with $q_0 = (3/4\pi)ZR_0^2$ with $R_0 = 1.2A^{\frac{1}{3}}$ fm. Using the experimental data given in Fig. 12, the values of $|\beta_2(0_1^+)| = 0.238(17)$ for the ground state, and $|\beta_2(0_2^+)| = 0.179(14)$ for the 0_2^+ state are found. In principle, these values represent lower limits. For the ground state, the sum is typically strongly dominated by the contribution from the $\langle 2_1^+\|E2\|0_1^+\rangle$ matrix element and hence it is unlikely to change significantly by extending it over more states. For the 0_2^+ state, the most important contribution to the sum is expected to arise from its coupling to the 2^+ rotational band member built on this state, and the contribution from the 2_1^+ state is usually important as well. If one assumes, following Ref. [20], that the 0_2^+ and 2_3^+ states form a rotational band, and that no other 2^+ states have enhanced $B(E2)$ values for the decay to the 0_2^+ state, the present result indicates that the deformation of the 0_2^+ state is significantly lower than that of the ground state. The convergence of the sum is supported by the observation that the next 2^+ state is located at 2037 keV and has no known decay branch to the 0_2^+ level. Similarly, while the $B(E2; 2_2^+ \to 0_2^+)$ value formally contributes to the $\langle Q^2\rangle$ value for the 0_2^+ state, this decay branch is unknown in ^{102}Ru, and in the neighboring ^{104}Ru the corresponding $B(E2)$ value was determined to be 0.4(3) W.u. [25]. Consequently, the present results are consistent with the 0_2^+ state in ^{102}Ru possessing a significantly lower deformation than the ground state, and

mirror the results obtained for ^{104}Ru [9,25] that also indicated that the 0_2^+ state was less deformed than the 0_1^+ state.

IV. CONCLUSIONS

Coulomb excitation of ^{102}Ru was performed with beams of ^{12}C and ^{16}O, and the scattered ions were analyzed with a magnetic spectrograph. The populations of the 2_1^+, 2_2^+, 2_3^+, 3_1^-, and 3_2^- states were extracted, and from them, using the Coulomb-excitation code GOSIA, $B(E\lambda)$ values were determined. The results for the 2_1^+ state were consistent with the evaluated $B(E2; 2_1^+ \to 0_1^+)$ value, whereas $B(E2; 2_2^+ \to 0_1^+)$ and $B(E3; 3_1^- \to 0_1^+)$ values were greater than the evaluated values. A peak attributed to the 2_3^+ level was observed in a single spectrum, enabling the first determination of the $B(E2; 0_1^+ \to 2_3^+)$ value. Using this result, and the spectroscopic data for the 2_3^+ level, the $B(E2; 2_3^+ \to 0_2^+)$ value is determined to be 18(4) W.u., substantially less than the $B(E2; 2_1^+ \to 0_1^+)$ value, suggesting that the 0_2^+ band has a lower quadrupole collectivity than the ground-state band. The rotational invariants $\langle Q^2\rangle$ extracted from the experimental data support this conclusion, leading to β_2 values of $\simeq 0.24$ for the ground state, and $\simeq 0.18$ for the 0_2^+ state. The experimental results are compared with symmetry-conserving configuration-mixing method calculations that generally overpredict the $E2$ transition rates.

The magnitude of the $B(E3; 3_1^- \to 0_1^+)$ value in ^{102}Ru, 31.5(35) W.u., is larger than the literature value. A recent measurement for ^{100}Mo also extracted a significantly larger $B(E3)$ value than those resulting from previous studies, suggesting that the $E3$ strengths should be reexamined in this mass region.

[1] H. G. Börner, R. F. Casten, M. Jentschel, P. Mutti, W. Urban, and N. V. Zamfir, Phys. Rev. C **84**, 044326 (2011).

[2] J. Stachel, P. Van Isacker, and K. Heyde, Phys. Rev. C **25**, 650 (1982).

[3] I. Stefanescu, A. Gelberg, J. Jolie, P. Van Isacker, P. von Brentano, Y. X. Luo, S. J. Zhu, J. O. Rasmussen, J. H. Hamilton, A. V. Ramayya, and X. L. Che, Nucl. Phys. A **789**, 125 (2007).

[4] A. Giannatiempo, A. Nannini, P. Sona, and D. Cutoiu, Phys. Rev. C **52**, 2969 (1995).

[5] J. L. M. Duarte, T. Borello-Lewin, G. Maino, and L. Zuffi, Phys. Rev. C **57**, 1539 (1998).

[6] H. Duckwitz, M. Pfeiffer, M. Albers, C. Bernards, C. Fransen, J. Jolie, P. Petkov, D. Radeck, T. Thomas, and K. O. Zell, Nucl. Phys. A **903**, 18 (2013).

[7] D. A. Arseniev, A. Sobiczewski, and V. G. Soloviev, Nucl. Phys. A **139**, 269 (1969).

[8] A. Faessler, J. E. Galonska, U. Götz, and H. C. Pauli, Nucl. Phys. A **230**, 302 (1974).

[9] J. Stachel, N. Kaffrell, E. Grosse, H. Emling, H. Folger, R. Kulessa, and D. Schwalm, Nucl. Phys. A **383**, 429 (1982).

[10] R. F. Casten, E. R. Flynn, O. Hansen, and T. J. Mulligan, Nucl. Phys. A **184**, 357 (1972).

[11] E. R. Flynn, F. Ajzenberg-Selove, R. E. Brown, J. A. Cizewski, and J. W. Sunier, Phys. Rev. C **24**, 2475 (1981).

[12] H. W. Fielding, R. E. Anderson, D. A. Lind, C. D. Zafiratos, and W. P. Alford, Nucl. Phys. A **269**, 125 (1976).

[13] D. Troltenier, J. A. Maruhn, W. Greiner, V. Velazquez Aguilar, P. O. Hess, and J. H. Hamilton, Z. Phys. A: Hadrons Nucl. **338**, 261 (1991).

[14] M. Sugita and A. Arima, Nucl. Phys. A **515**, 77 (1990).

[15] K. Nomura, R. Rodríguez-Guzmán, and L. M. Robledo, Phys. Rev. C **94**, 044314 (2016).

[16] H. Abusara, S. Ahmad, and S. Othman, Phys. Rev. C **95**, 054302 (2017).

[17] Z. Shi and Z. P. Li, Phys. Rev. C **97**, 034329 (2018).

[18] G. Lévai and J. M. Arias, Phys. Rev. C **81**, 044304 (2010).

[19] A. Jalili Majarshin and H. Sabri, Nucl. Phys. A **964**, 69 (2017).

[20] W. Urban, M. Jentschel, R. F. Casten, J. Jolie, Ch. Bernards, B. Maerkisch, Th. Materna, P. Mutti, L. Próchniak, T. Rząca-Urban, G. S. Simpson, V. Werner, and S. Ahmed, Phys. Rev. C **87**, 031304(R) (2013).

[21] P. E. Garrett, L. Makhathini, R. A. Bark, T. R. Rodríguez, S. Valbuena, V. Bildstein, T. D. Bucher, C. Burbadge, R. Dubey, T. Faestermann, R. Hertenberger, M. Kamil, E. A. Lawrie, K. G. Leach, A. D. MacLean, C. Mehl, S. H. Mthembu, N. J. Mukwevho, C. Ngwetsheni, S. S. Ntshangase, J. C. Nzobadila Ondze, J. N. Orce, B. Rebeiro, B. Singh, S. Triambak, E. C. Vyfers, and H.-F. Wirth, Phys. Lett. B **809**, 135762 (2020).

[22] P. E. Garrett, L. Makhathini, R. A. Bark, T. R. Rodríguez, S. Valbuena, V. Bildstein, T. D. Bucher, C. Burbadge, R. Dubey, T. Faestermann, R. Hertenberger, M. Kamil, E. A. Lawrie, K. G. Leach, A. D. MacLean, C. Malotana, C. Mehl, S. H. Mthembu, J. Mukwevho, C. Ngwetsheni, S. S. Ntshangase, J. Ondze, J. N. Orce, B. Rebeiro, B. Singh, S. Triambak, E. C. Vyfers, and H.-F. Wirth, Acta Phys. Pol., B **51**, 799 (2020).

[23] M. Zielińska, T. Czosnyka, J. Choiński, J. Iwanicki, P. Napiorkowski, J. Srebrny, Y. Toh, M. Oshima, A. Osa, Y. Utsuno, Y. Hatsukawa, J. Katakura, M. Koizumi, M. Matsuda, T. Shizuma, M. Sugawara, T. Morikawa, H. Kusakari, A. D. Efimov, and V. M. Mikhajlov, Nucl. Phys. A **712**, 3 (2002).

[24] K. Wrzosek-Lipska, L. Próchniak, M. Zielińska, J. Srebrny, K. Hadyńska-Klęk, J. Iwanicki, M. Kisieliński, M. Kowalczyk, P. J. Napiorkowski, D. Piętak, and T. Czosnyka, Phys. Rev. C **86**, 064305 (2012).

[25] J. Srebrny, T. Czosnyka, Ch. Droste, S. G. Rohoziński, L. Próchniak, K. Zając, K. Pomorski, D. Cline, C. Y. Wu, A. Bäcklin, L. Hasselgren, R. M. Diamond, D. Habs, H. J. Körner, F. S. Stephens, C. Baktash, and R. P. Kostecki, Nucl. Phys. A **766**, 25 (2006).

[26] R. Arnold, C. Augier, A. S. Barabash, A. Basharina-Freshville, S. Blondel, S. Blot, M. Bongrand, D. Boursette, V. Brudanin, J. Busto *et al.*, Eur. Phys. J. C **79**, 440 (2019).

[27] A. S. Barabasha, F. T. Avignone, III, J. I. Collar, C. K. Guerard, R. J. Arthur, R. L. Brodzinski, H. S. Miley, J. H. Reeves, J. R. Meier, K. Ruddick, and V. I. Umatov, Phys. Lett. B **345**, 408 (1995).

[28] B. Lehnert, K. Zuber, E. Andreotti, and M. Hult, Phys. Rev. C **87**, 034312 (2013).

[29] J. Engel and J. Menéndez, Rep. Prog. Phys. **80**, 046301 (2017).

[30] C. S. Lim, W. N. Catford, and R. H. Spear, Nucl. Phys. A **522**, 635 (1991).

[31] W. A. Mayer, J. Koenig, H. J. Körner, D. Pereira, K. E. Rehm, and H.-J. Scheerer, *Jahresbericht BL 1980*, p. 142 (1981).

[32] C. Albrecht, T. Faestermann, A. Gillitzer, F. Heine, and R. Schneider, *Jahresbericht BL 1993* (1994), p. 188.

[33] D. De Frenne, Nucl. Data Sheets **110**, 1745 (2009).

[34] C. Fahlander, L. Hasselgren, J. E. Then, A. Bockisch, A. M. Kleinfeld, A. Gelberg, and K. P. Lieb, Phys. Lett. B **60**, 347 (1976).

[35] M. P. Fewell, D. C. Kean, R. H. Spear, and A. M. Baxter, J. Phys. G: Nucl. Phys. **3**, L27 (1977).

[36] M. T. Esat, D. C. Kean, R. H. Spear, M. P. Fewell, and A. M. Baxter, Phys. Lett. B **72**, 49 (1977).

[37] R. H. Spear, T. H. Zabel, A. M. Baxter, M. P. Fewell, S. Hinds, A. M. R. Joye, and D. C. Kean, Aust. J. Phys. **31**, 377 (1978).

[38] M. P. Fewell, R. H. Spear, T. H. Zabel, and A. M. Baxter, Aust. J. Phys. **33**, 505 (1980).

[39] R. H. Spear and M. P. Fewell, Aust. J. Phys. **33**, 509 (1980).

[40] M. T. Esat, M. P. Fewell, R. H. Spear, T. H. Zabel, A. M. Baxter, and S. Hinds, Nucl. Phys. A **362**, 227 (1981).

[41] R. H. Spear, T. H. Zabel, M. T. Esat, A. M. Baxter, and S. Hinds, Nucl. Phys. A **378**, 559 (1982).

[42] W. J. Vermeer, M. T. Esat, and R. H. Spear, Nucl. Phys. A **389**, 185 (1982).

[43] W. J. Vermeer, M. T. Esat, J. A. Kuehner, R. H. Spear, A. M. Baxter, and S. Hinds, Phys. Lett. B **122**, 23 (1983).

[44] T. Czosnyka, D. Cline, and C. Y. Wu, Bull. Am. Phys. Soc. **28**, 745 (1983).

[45] I. J. Thompson, Comput. Phys. Rep. **7**, 167 (1988).

[46] M. C. Mermaz, J. C. Peng, N. Lisbona, and A. Greiner, Phys. Rev. C **15**, 307 (1977).

[47] L. Gan, Z.-H. Li, H.-B. Sun, Sh.-P. Hu, E.-T. Li, and J. Zhongu, Chin. Phys. C **45**, 054105 (2021).

[48] Y.-L. Xu, Y.-L. Han, X.-W. Sun, X.-J. Sun, H.-Y. Liang, H.-R. Guo, and Ch.-H. Cai, Chin. Phys. C **44**, 124103 (2020).

[49] T. Kibédi and R. H. Spear, Atom. Data Nucl. Data Tables **80**, 35 (2002).

[50] F. K. McGowan, R. L. Robinson, P. H. Stelson, and W. T. Milner, Nucl. Phys. A **113**, 529 (1968).

[51] A. Bockisch, M. Miller, A. M. Kleinfeld, A. Gelberg, and U. Kaup, Z. Phys. A: At. Nucl. (1975) **292**, 265 (1979).

[52] S. Landsberger, R. Lecomte, P. Paradis, and S. Monaro, Phys. Rev. C **21**, 588 (1980).

[53] T. R. Rodríguez and J. L. Egido, Phys. Rev. C **81**, 064323 (2010).

[54] R. N. Bernard, L. M. Robledo, and T. R. Rodríguez, Phys. Rev. C **93**, 061302(R) (2016).

[55] M. Borrajo, T. R. Rodríguez, and J. L. Egido, Phys. Lett. B **746**, 341 (2015).

[56] G. A. Lalazissis, T. Nikšić, D. Vretenar, and P. Ring, Phys. Rev. C **71**, 024312 (2005).

[57] T. Nikšić, D. Vretenar, and P. Ring, Phys. Rev. C **78**, 034318 (2008).

[58] P. W. Zhao, Z. P. Li, J. M. Yao, and J. Meng, Phys. Rev. C **82**, 054319 (2010).

[59] T. Kibédi, A. B. Garnsworthy, and J. L. Wood, Prog. Part. Nucl. Phys. **123**, 103930 (2022).

[60] D. Cline, Annu. Rev. Nucl. Part. Sci. **36**, 683 (1986).